Supporting Information

Heller et al. 10.1073/pnas.1005512108

SI Methods

Preparation of Biopolymer-Encapsulated Single-Walled Carbon Nanotubes (SWNT) Bombolitin peptide–SWNT was prepared by combining bombolitin peptide with SWNT prepared by the high-pressure CO conversion (HiPCO) method (Unidym) in a 2:1 mass ratio in 20 mM Tris and 100 mM NaCl (henceforth known as Tris buffer) using a one-eighth-inch probe-tip sonicator (Vibra-Cell) at 10 W for 10 min. The resulting bombolitin–SWNT solution was centrifuged twice for 90 min at $16{,}300 \times g$ and the pellet removed each time.

SWNT encapsulated by a single-stranded DNA oligonucleotide with the sequence $(AT)_{15}$ [ss$(AT)_{15}$] was prepared by sonicating nanotubes (Nano-C or Unidym) in the presence of ss$(AT)_{15}$ DNA (Integrated DNA Technologies) in a 2:1 DNA:SWNT ratio in a solution of 0.1 M NaCl using the same sonication and centrifugation steps as detailed in the text.

Suspensions of SWNT encapsulated by poly(vinyl alcohol) (PVA) were prepared by first sonicating nanotubes in the presence of a 2% aqueous solution of sodium cholate for 20 min in a 750-W cup-horn sonicator (Vibra-Cell) at 90% amplitude. Suspensions were ultracentrifuged for 4 h at $100{,}000 \times g$ and the pellet removed. The resulting suspension was stirred with 2% PVA (31,000–50,000 MW) overnight at 70 °C then dialyzed against 2 L of water for 24 h.

Preparation of Cyclotrimethylenetrinitramine (RDX) Solutions. A mixture of 10:1 weight ratio sand to RDX (XM Division, Van Aken International) was extracted with acetonitrile and filtered. A saturated aqueous solution of RDX was prepared by dissolving 1:100 in water and centrifuging twice at $16{,}300 \times g$ for 3 min; the pellet was removed each time.

High-Throughput Analyte Screening. Analyte screening was conducted in a 96-well plate containing a bombolitin-II–SWNT solution with 8 uM of peptide, PVA–SWNT solution of 2 mg/L SWNT, or ss$(AT)_{15}$–SWNT solution of 0.5–1 mg/L SWNT. The SWNT solutions were interrogated by the analytes added separately to each well, incubated for 1 h, and measured via near-infrared (NIR) photoluminescence (PL) spectroscopy with 785-nm excitation on a microscope with automated translation stage. Spectra were fit to a series of eight Lorentzian peaks to give analyte responses of each (n,m) SWNT species. Concentrations of analytes are listed in supporting tables.

Bombolitin-II–RDX Absorption Spectroscopy. Bombolitin-II–SWNT with a concentration of 80 μM bombolitin II was suspended in Tris buffer, 90 μM RDX, and 0.5% acetonitrile. A control sample contained bombolitin-II–SWNT, Tris, and acetonitrile only.

SDS Addition Experiment. Bombolitin–SWNT solutions containing 44 μM bombolitin II in Tris buffer were aliquoted in a well plate and mixed with varying concentrations of SDS. NIR PL spectra were acquired 1 h after mixing.

Circular Dichroism. CD measurements were obtained using an Aviv Model 202 CD Spectrometer in a 1-mm path length strain-free cuvette. Bombolitin solutions of 0.275 mM in Tris buffer were measured before and after the addition of 9 μM of RDX in 1% acetonitrile while keeping the bombolitin and acetonitrile concentrations constant. Background spectra of Tris/acetonitrile and Tris/RDX/acetonitrile were subtracted from the control and RDX-interacting spectra of peptides, respectively.

Computational Study of Bombolitin-II–RDX Binding. The bombolitin II and RDX structures were drawn in HyperChem and subsequently optimized using the Model Build function. Both structures were energetically relaxed using the Hyperchem software "geometry optimize" function based on periodic boundary conditions. Bombolitin II and RDX were centered within a $56 \times 56 \times 56$-Å periodic box containing a maximum of 5,833 water molecules, with the minimum distance between the solvent and solute molecules set at 2.3 Å. The Polak-Ribiere (conjugate gradient) algorithm was used with a termination criteria of an rms gradient of >0.1 kcal/Å mol, or 32,767 cycles. Net free energy of binding was determined by separately computing bombolitin II and RDX energies both in the interacting and noninteracting conditions.

Trinitrotoluene (TNT) Binding Experiments. A solution of 1 mg/L ss$(AT)_{15}$–SWNT in Tris buffer was interrogated with TNT dissolved in acetonitrile (Sigma) and measured 30 min to 1 h after mixing. Acetonitrile concentrations in the control were varied to equal experimental samples. For absorption spectroscopy, a spectrum with 44 μM TNT in Tris and 1% acetonitrile was subtracted from the SWNT–TNT spectrum to account for the absorption of the TNT molecule. A control spectrum of acetonitrile was subtracted from spectra used for the adsorption isotherm.

Microscopy of RDX-Induced Bombolitin-II–SWNT Solvatochromic Shifts. As-produced bombolitin-II–SWNT were deposited on a glass-bottom Petri dish (MatTek Corporation) for 15–30 min, rinsed three times with Tris buffer, and left with 100 μL Tris buffer covering the glass-bound nanotubes. The imaging buffer included an aliquot of 8 μM of bombolitin II peptide. Movies were collected at 1 s/frame. An aliquot of 100 μL of 18 μM RDX suspended in Tris buffer was added to the Petri dish 100 s after data collection began, resulting in a final concentration of 9 μM. The path was modified by the optical setup illustrated in Fig. 4. Spots of 2×2 pixels on the two channels were correlated by translating the region of interest by a constant x value. Intensity time-trace information of the top 100 highest-intensity spots on the short-λ channel, along with their long-λ channel complements, was collected. Time traces were fit with an iterative error-minimizing step-finding algorithm described by Kerssemakers et. al (1).

Microscopy of TNT-Induced Quenching of ss$(AT)_{15}$–SWNT A solution of ss$(AT)_{15}$ DNA–SWNT was incubated on a glass-bottom Petri dish (MatTek Corporation) for 15–30 min, rinsed three times with Tris buffer, and left with 100 μL Tris buffer covering the glass-bound nanotubes. Nanotubes were excited with a 658-nm laser. Movies at 500 ms/frame of the PL of the bound SWNT were taken with a 256×320 pixel InGaAs array detector (PI Acton) coupled to a Zeiss Axio Observer D1 microscope. An aliquot of 100 μL TNT suspended in Tris buffer was added to the glass 100 frames after data collection began. Data were processed by obtaining 100 time traces of 2×2 pixel regions with the highest intensities in the image field. Movies containing at least one discrete step were processed by fitting the trace of each nanotube spot's intensity vs. time to an idealized trace using iterative application of an error-minimization algorithm (1). A histogram of quenching/dequenching step heights was constructed by compiling all fitted steps from one movie in which 1.1 μM of TNT was introduced. The histogram was subsequently fitted by a series of five Gaussian curves using an algorithm taken from a collection of fitting functions written for Matlab.

Calculating Forward and Reverse Rate Constants of Single-Molecule TNT Binding Traces. Forward and reverse rate constants were fit using the birth-and-death population modeling approach (2). A quenching event is treated as a "death" with a death rate of k_f, and a dequenching event is treated as a "birth" with a birth rate of k_r. The florescence value of a nanotube at any given time point is equivalent to the total population at that time. A nanotube is at a florescence state i at a given time t_0; the probability that it will be at state j at time $t + \Delta t$ is dependent on whether the final state j is a dequenched state ($j = i + 1$), a quenched state ($j = i - 1$), or an unchanged state ($j = i$):

$$P(\text{intensity}_{t_0+\Delta t} = j | \text{intensity}_{t_0} = i) = \begin{Bmatrix} (I_{\max} - i)k_r\Delta t & \text{if } j = i+1 \\ 1 - (I_{\max} - i)k_r\Delta t - ik_f\Delta t & \text{if } j = i \\ ik_f\Delta t & \text{if } j = i-1 \end{Bmatrix} \quad [S1]$$

where $I_{\max}$ is the maximum possible value of the intensity. Based on this model, expressions for this forward and reverse rate constants become

$$k_f = \frac{N_{\text{quenched}}}{S_t} \quad [S2]$$

$$k_r = \frac{N_{\text{dequenched}}}{I_{\max}t - S_t}, \quad [S3]$$

where N_{quenched} is the number of instances the trace undergoes a quenching step, $N_{\text{dequenched}}$ is the number of instances the trace undergoes a dequenching step, t is the total time of the trace, and S_t is the sum of all the times of all the unquenched sites throughout trace time interval of [0, t]

$$S_t = \int_0^t I_x dx, \quad [S4]$$

where I_x is the instantaneous intensity at time x.

Discussion of SDS Experiments. The native conformation of the bombolitin II peptide in aqueous solution is largely unordered, although some structure exists given the broad shoulder at 222 nm in the CD spectrum. Upon introduction of low concentrations of SDS to the peptide, β-aggregates form in solution (3, 4). At concentrations near the critical micelle concentration, the peptide suspends in solution and adopts an α-helical conformation, which was demonstrated in the presence of the nanotube by addition of SDS to the bombolitin-II–SWNT suspension (Fig. S3). Upon addition of 80 uM SDS to 45 μM peptide, the nanotube PL falls and shifts drastically, and precipitates are visible, which compares favorably with CD data in the literature. This result shows a distinct change in ellipticity of the peptide perturbed with SDS at the same concentration ratio (5). The SWNT intensity increases and blue-shifts at higher SDS concentrations, but it is not clear whether this was caused by the resuspension of the peptide or the direct suspension of nanotubes by SDS. Regardless, this experiment demonstrates the high sensitivity of nanotube PL to the bombolitin II conformation.

1. Kerssemakers JWJ, et al. (2006) Assembly dynamics of microtubules at molecular resolution. *Nature* 442:709–712.
2. Keiding N (1975) Maximum likelihood estimation in birth-and-death process. *Ann Stat* 3:363–372.
3. Peggion E, Mammi S, Schievano E (1997) Conformation and interactions of bioactive peptides from insect venoms: The bombolitins. *Biopolymers* 43:419–431.
4. Schievano E, Mammi S, Monticelli L, Ciardellaj M, Peggion E (2003) Conformational studies of a bombolitin III-derived peptide mimicking the four-helix bundle structural motif of proteins. *J Am Chem Soc* 125:15314–15323.
5. Battistutta R, Pastore A, Mammi S, Peggion E (1995) Conformational properties of the amphipathic lytic polypeptide bombolitin II—a circular-dichroism, NMR and computer-simulation study. *Macromol Chem Phys* 196:2827–2841.

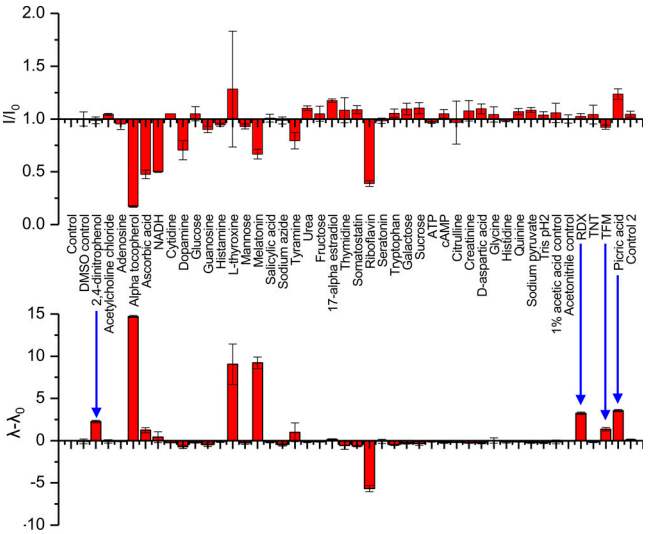

Fig. S1. Intensity (*Upper*) and wavelength (*Lower*) responses of bombolitin-II–SWNT PL on exposure to 42 analytes and controls. Intensity response (*Upper*) is normalized with respect to control intensity (I/I_0). Wavelength shifting response (*Lower*) is presented as the peak wavelength in nanometers subtracted from that of the control (λ-λ_0). Certain nitro group compounds elicit PL shifting with little concomitant quenching (blue arrows). (All error bars indicate one standard deviation.) TFM, 4-nitro-3(trifluoromethyl)phenol.

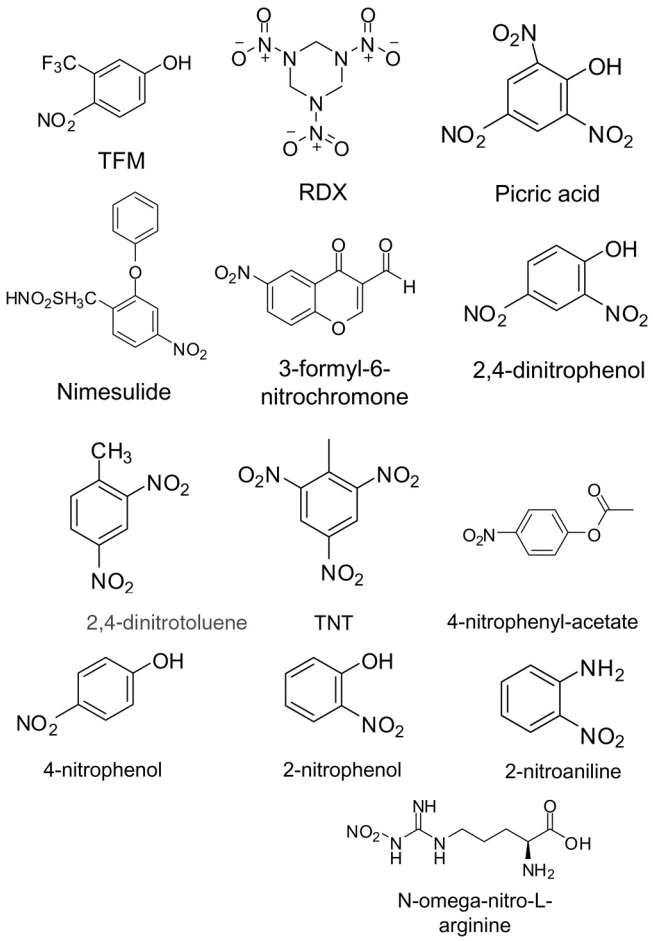

Fig. S2. Nitro group-containing compounds exposed to bombolitin-II–SWNT. TFM, 4-nitro-3(trifluoromethyl)phenol.

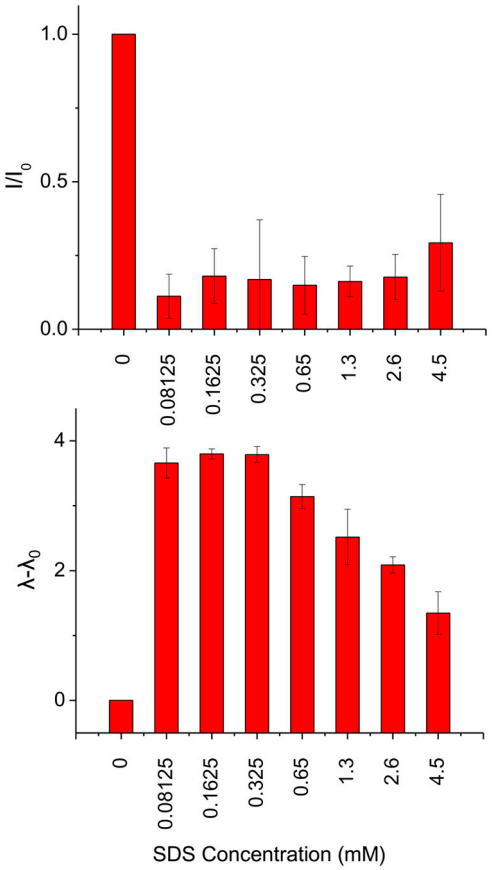

Fig. S3. Bombolitin-II–SWNT PL changes upon addition of SDS. Variations in the intensity (*Upper*) and wavelength (*Lower*) of the (11,3) SWNT species are shown after 6 h of equilibration in a well plate.

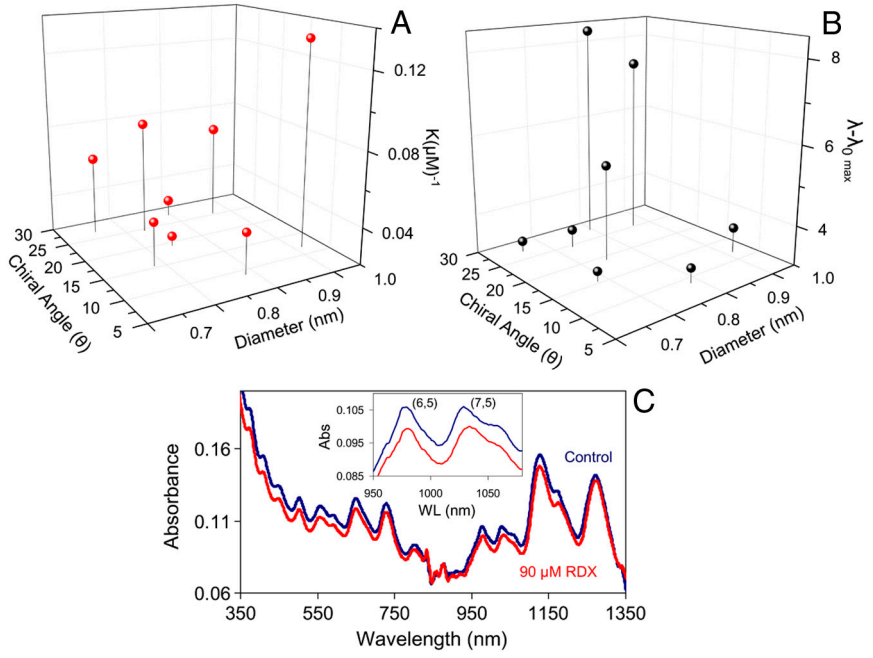

Fig. S4. (*A*) Langmuir equilibrium constants in inverse micromolar of individual SWNT species plotted versus nanotube chiral angle and diameter from RDX-induced shifting of bombolitin-II–SWNT emission. (*B*) Maximum value of the RDX-induced nanotube emission wavelength shift from the same experiment plotted versus nanotube chiral angle and diameter. (*C*) Absorption spectra of bombolitin-II–SWNT before (blue) and after (red) introducing 90 μM RDX. The absorbance drops slightly and wavelength shifts to different degrees depending on the (n,m) species of the nanotube. The (7,5) nanotube shifts approximately 5 nm. (*Inset*) Enlargement of 950–1,080 nm region.

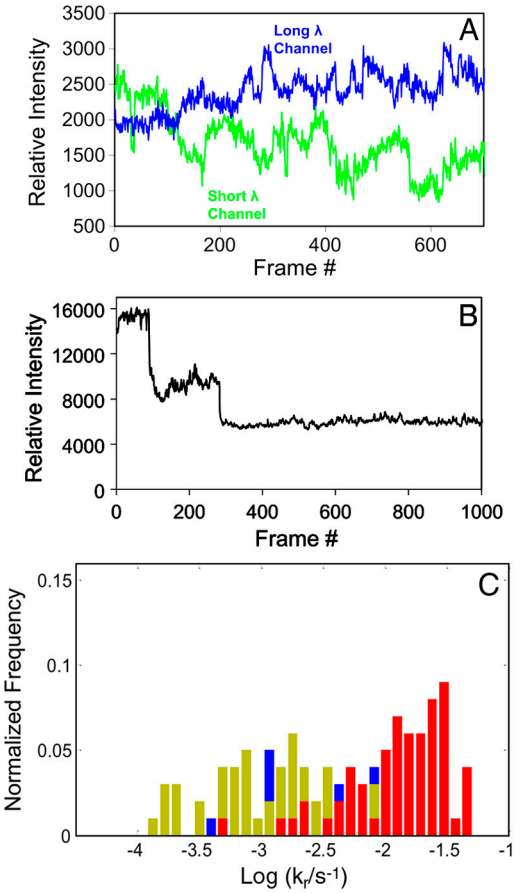

Fig. S5. (*A*) Nonnormalized intensity trace of surface-adsorbed bombolitin-II–SWNT PL data taken with the split-channel microscope, corresponding to the normalized trace in Fig. 4*E*. (*B*) Nonnormalized intensity trace of surface-adsorbed ss(AT_{15})–SWNT upon introduction of TNT, corresponding to the normalized trace in Fig. 6*D*. (*C*) Histogram of reverse quenching (dequenching) rates of nanotubes corresponding to the forward rate histogram in Fig. 6*F*. Nanotubes were exposed to 0.22 μM (blue), 1.1 μM (gold), and 2.2 μM (red) of TNT.

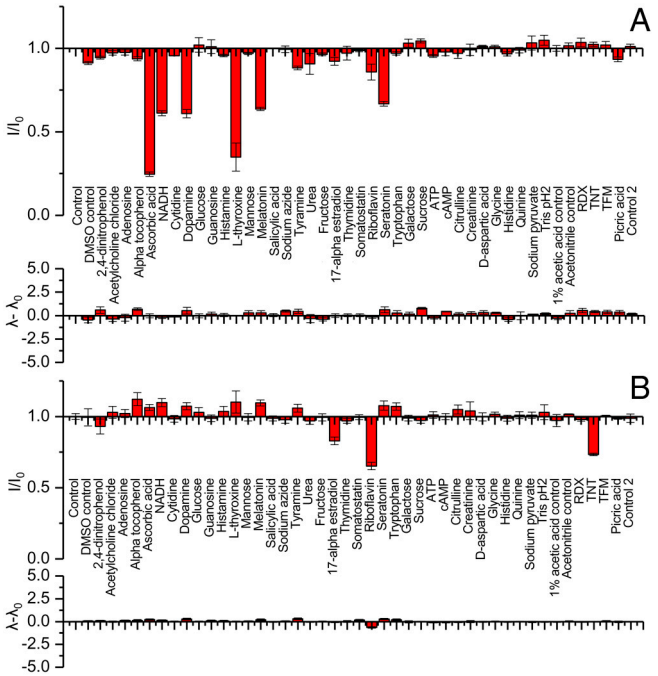

Fig. S6. Intensity changes and wavelength shifts of the (7,5) nanotube species in response to 42 analytes and controls for (*A*) PVA–SWNT and (*B*) ss(AT_{15})–SWNT. TFM, 4-nitro-3(trifluoromethyl)phenol.

Table S1. List of 42 analytes, controls, and concentrations of each analyte used for high-throughput screening

Compound	Conc.
Control	—
DMSO control	1%
2,4-dinitrophenol	480
Acetylcholine chloride	540
Adenosine	510
Alpha tocopherol	510
Ascorbic acid	500
NADH	510
Cytidine	480
Dopamine	490
Glucose	10,890
Guanosine	510
Histamine	510
L-thyroxine	100
Mannose	10,300
Melatonin	490
Salicylic acid	490
Sodium azide	510
Tyramine	490
Urea	490
Fructose	10,800
17-α-estradiol	99
Thymidine	520
Somatostatin	6
Riboflavin	100
Seratonin	110
Tryptophan	250
Galactose	5,000
Sucrose	100
ATP	110
cAMP	96
Citrulline	110
Creatinine	98
D-aspartic acid	20
Glycine	500
Histidine	99
Quinine	10
Sodium pyruvate	500
Tris, pH 2	—
Acetic acid control	1%
Acetonitrile control	1%
RDX	90
TNT	22
4-nitro-3-(trifluoromethyl)phenol	118
Picric acid	28
Control 2	—

Concentrations are listed in micromolar unless otherwise noted.

Table S2. List of 13 nitro group-containing analytes, controls, and concentrations of each analyte

Compound	Conc.
Control	0
Acetonitrile control	1%
DMSO control	1%
Picric acid	28.35
TNT	22.02
RDX	90
4-nitro-3-(trifluoromethyl)phenol	99.46
2,4-dinitrophenol	100
4-nitrophenyl acetate	100
N-ω-nitro-L-arginine	97.17
2-nitroaniline	99.9
3-formyl-6-nitrochromone	84.9
Nimesulide	100.55
2-nitrophenol	100
2,4-dinitrotoluene	106.47
4-nitrophenol	104.23

Concentrations are listed in micromolar unless otherwise noted.

Table S3. Loadings for principal component analysis plot in Fig. 2

Input Variable		PC1	PC2	PC3
(8,3)	Intensity	0.0247	0.0220	−0.0049
(6,5)	Intensity	0.0133	0.0170	−0.0010
(7,5)	Intensity	0.0197	0.0257	0.0090
(10,2)	Intensity	0.0176	0.0247	−0.0397
(8,4)	Intensity	0.0212	0.0163	−0.0128
(7,6)	Intensity	0.0245	0.0262	−0.0323
(8,6)	Intensity	0.0197	−0.0033	0.0104
(11,3)	Intensity	0.0346	−0.0649	0.0105
(8,3)	Wavelength	−0.2348	0.0212	−0.0073
(6,5)	Wavelength	−0.0851	0.2712	−0.1581
(7,5)	Wavelength	−0.1972	0.0048	−0.6714
(10,2)	Wavelength	−0.4291	−0.0853	0.4189
(8,4)	Wavelength	−0.3753	0.0957	0.4816
(7,6)	Wavelength	−0.6703	−0.4663	−0.2561
(8,6)	Wavelength	−0.3095	0.6836	−0.1913
(11,3)	Wavelength	−0.1567	0.4664	0.1071